AGU PUBLICATIONS

Geophysical Research Letters

RESEARCH LETTER
10.1002/2015GL067172

Key Points:
- An analytic model for high-latitude temperature profiles is derived
- Sensitivity of temperature profiles depends on the nature of the forcing
- The model may be useful for study of paleoclimate and exoplanet atmospheres

Correspondence to:
T. W. Cronin,
timothywcronin@fas.harvard.edu

Citation:
Cronin, T. W., and M. F. Jansen (2015), Analytic radiative-advective equilibrium as a model for high-latitude climate, *Geophys. Res. Lett.*, *42*, doi:10.1002/2015GL067172.

Received 25 NOV 2015
Accepted 10 DEC 2015
Accepted article online 14 DEC 2015

Analytic radiative-advective equilibrium as a model for high-latitude climate

Timothy W. Cronin[1] and Malte F. Jansen[2]

[1]Department of Earth and Planetary Sciences, Harvard University, Cambridge, Massachusetts, USA, [2]Department of the Geophysical Sciences, University of Chicago, Chicago, Illinois, USA

Abstract We propose radiative-advective equilibrium as a basic-state model for the high-latitude atmosphere. Temperature profiles are determined by a competition between stabilization by atmospheric shortwave absorption and advective heat flux convergence, and destabilization by surface shortwave absorption. We derive analytic expressions for temperature profiles, assuming power law atmospheric heating profiles as a function of pressure and two-stream windowed-gray longwave radiative transfer. We discuss example profiles with and without an atmospheric window and show that the sensitivity of surface temperature to forcing depends on the nature of the forcing, with greatest sensitivity to radiative forcing by increased optical thickness and least sensitivity to increased atmospheric heat transport. These differences in sensitivity of surface temperature to forcing can be explained in terms of a forcing-dependent lapse-rate feedback.

1. Introduction

In this paper, we seek to understand the vertical temperature structure, or lapse rate, of the high-latitude troposphere. The high-latitude lapse rate typically increases with warming, and has been found to play a large role in polar amplification of climate change [*Pithan and Mauritsen*, 2014]. Particularly challenging—and critical for the determination of high-latitude surface temperatures and their sensitivity to climate change—is the lapse rate in the lower troposphere and boundary layer, which is highly stable and has frequent surface-based inversions, especially in winter (Figure 1).

The vertical temperature structure at high latitudes is more stable and less well understood than the vertical temperature structure in midlatitudes and in the tropics. Earth's tropics can be approximated well by radiative-convective equilibrium: heating from moist convection balances radiative cooling, and the lapse rate of the troposphere closely follows a moist adiabat [*Xu and Emanuel*, 1989; *Sobel et al.*, 2001]. Although radiative-convective equilibrium provides a good basic state for the tropics, the extratropical troposphere is typically stable to moist convection, so different dynamics must be invoked to understand the lapse rate there. *Stone* [1978] and *Stone and Carlson* [1979] proposed that a simple marginal criticality condition to baroclinic instability links the meridional and vertical temperature gradients in the extratropics (amounting to a nonlocal constraint on the lapse rate). Recent work has pointed to limitations of the marginal criticality condition but supports the idea that the extratropical lapse rate is modulated by baroclinic eddy fluxes and depends nonlocally on the vertical and horizontal structure of the radiative forcing [*Jansen and Ferrari*, 2013]. Although these arguments have proven useful for understanding the bulk midlatitude meridional temperature gradient and static stability, they are difficult to apply locally and at higher latitudes. Thus, we still lack a theoretical understanding of the high-latitude lapse rate and how it interacts with different forcings and feedbacks.

This article presents an analytic radiative-advective equilibrium model for the high-latitude lapse rate. Profiles result from a competition between the stabilizing influences of atmospheric solar absorption and prescribed advective heat flux convergence and the destabilizing influences of surface solar absorption and subsurface heating. This work builds off of previous studies that have assumed a similar balance between radiative cooling and prescribed advective heating [*Overland and Guest*, 1991; *Abbot and Tziperman*, 2008; *Payne et al.*, 2015], but we simplify the treatment of heat transfer to obtain analytic solutions with a continuous vertical coordinate.

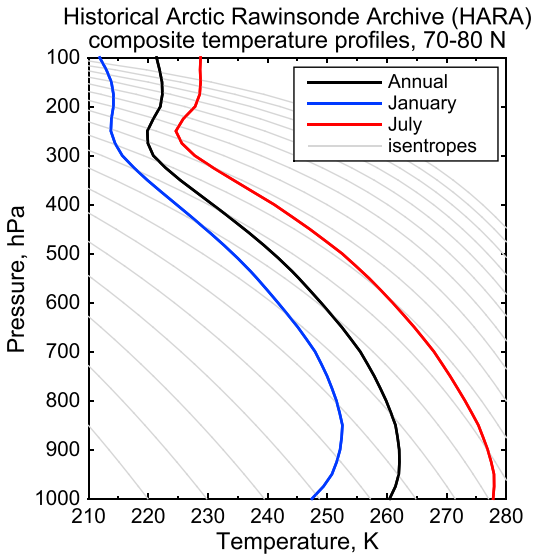

Figure 1. Composite of high-latitude temperature profiles for January (blue), July (red), and annual mean (solid black), based on Historical Arctic Rawindsonde Archive (HARA) data, using all soundings between 1948–1996 and 70–80N that have no missing data [*Kahl et al.*, 1992; *Kahl and Serreze*, 2003]. Moist isentropes, or lines of constant θ_e, are contoured every 10 K from bottom left to top right (faint gray lines).

2. Derivation

We apply surface and atmospheric heat sources to an atmospheric column with two-stream longwave windowed-gray radiative transfer. The windowed-gray equations follow *Weaver and Ramanathan* [1995]: the atmosphere is characterized by a total infrared optical thickness τ_0 within a wide band occupying $(1-\beta)$ of the Planck-weighted thermal spectrum. In the remaining fraction β of the spectrum—the window—the atmosphere is completely transparent to infrared emission, and radiation escapes from the surface directly to space. This approximation is useful because it captures the ability of the surface to cool directly to space even when the atmosphere is optically thick across most of the spectrum and because it allows for analytic solutions to the equations of radiative transfer. Note that the assumption of fixed window width is highly idealized and does not account for increasing size of windows as pressure decreases, especially if a condensable gas (like water vapor) is a major source of infrared opacity.

We denote the surface solar absorption plus heating from subsurface heat flux convergence as F_S, and the total atmospheric moist static energy flux convergence plus solar atmospheric heating as F_A (both in W m^{-2}). We assume that the variation of optical thickness τ with pressure p follows a power law [*Pollack*, 1969]:

$$\tau = \tau_0 (p/p_0)^n. \tag{1}$$

Unless otherwise specified, we follow *Robinson and Catling* [2012] and assume that pressure-broadening dominates so that $n = 2$. Both pressure and optical thickness increase downward, to maximum values of p_0 and τ_0 at the surface. As in *Pierrehumbert* [2010], we consider all values of optical thickness to be prescaled by a geometric diffusivity factor D (usually taken between 3/2 and 2), relating to the hemispheric integration of radiance. This means that our choices of τ and τ_0 should be compared to values of $D\tau$ or $D\tau_0$ from other work [*Weaver and Ramanathan*, 1995; *Robinson and Catling*, 2012].

We must also impose vertical structure to the atmospheric shortwave and advective heating Q_A, which integrates to F_A in either pressure or optical thickness coordinates:

$$F_A = \int_0^{p_0} Q_A(p)\mathrm{d}p = \int_0^{\tau_0} Q_A(\tau)\mathrm{d}\tau. \tag{2}$$

We assume a power law distribution for the cumulative heating of the atmosphere above optical thickness τ:

$$\int_0^{\tau} Q_A(\tau')\mathrm{d}\tau' = F_A(\tau/\tau_0)^b, \tag{3}$$

so that differential heating rates in optical thickness and pressure coordinates are given by

$$Q_A(\tau) = bF_A/\tau_0(\tau/\tau_0)^{b-1} \tag{4}$$

$$Q_A(p) = nbF_A/p_0(p/p_0)^{nb-1}. \tag{5}$$

Two particularly simple cases are $b = 1$, for which heating is uniformly distributed in optical thickness, and $b = 1/2$, for which heating is uniformly distributed in pressure (recall that we generally take $n = 2$). The power law formulation of the heating rate is mathematically expedient and provides a versatile representation of the vertical structure of atmospheric heat transport. The power law profile in pressure translates into an exponential profile in altitude, with a decay scale $H_Q = H_p/(nb)$, where H_p is the pressure scale height of the atmosphere. *Chai and Vallis* [2014] argue that the vertical structure of heat flux in Charney-type baroclinic instability [*Charney*, 1947] can be approximated by an exponential with a decay scale $H_Q \lessapprox H_p/2$ for Earth-like parameters; though their fully nonlinear (dry) numerical simulations suggest weaker vertical decay at higher latitudes, justifying $nb \approx 1-2$. (Notice that the discussion in *Chai and Vallis* [2014] focusses on the temperature flux, which needs to be multiplied by the density to obtain an energy flux per unit height.) In warmer climates, where latent heat transport to high latitudes may dominate, the vertical decay scale may instead approximate the water vapor scale height, leading to a more bottom-heavy heating profile with $nb \approx 4$ [e.g. *Weaver and Ramanathan*, 1995].

We use the two-stream Schwartzchild equations for windowed-gray infrared radiative transfer:

$$\begin{aligned} \frac{\mathrm{d}F_1^+}{\mathrm{d}\tau} &= F_1^+ - (1-\beta)\pi B \\ \frac{\mathrm{d}F_1^-}{\mathrm{d}\tau} &= -F_1^- + (1-\beta)\pi B \\ \pi B(\tau) &= \sigma T^4(\tau), \end{aligned} \tag{6}$$

where F_1^+ is the upward infrared radiative flux, F_1^- is the downward infrared radiative flux, and B is the integrated Planck function [*Weaver and Ramanathan*, 1995]. These equations apply for a broad band of the spectrum that contains a fraction $(1-\beta)$ of the total thermal emission; the 1 subscript indicates fluxes within this band (as in the $_S$ subscript of *Weaver and Ramanathan* [1995], but note that their F_S must be multiplied by $(1-\beta)$ to yield a total flux).

It is useful to reframe equation (6) in terms of the within-band net flux F_1 and total intensity I_1, which are given by $F_1 = F_1^+ - F_1^-$ and $I_1 = F_1^+ + F_1^-$, and obey:

$$\frac{\mathrm{d}F_1}{\mathrm{d}\tau} = I_1 - 2(1-\beta)\pi B \tag{7}$$

$$\frac{\mathrm{d}I_1}{\mathrm{d}\tau} = F_1. \tag{8}$$

The net all-spectrum flux $F = F_1 + \beta\sigma T_S^4$ is known from the combined advective and shortwave heating profile (equation (3)):

$$F = F_1 + \beta\sigma T_S^4 = F_S + F_A\left[1 - (\tau/\tau_0)^b\right] \tag{9}$$

The boundary condition of no downward infrared flux at the top of the atmosphere ($F^-(0) = F_1^-(0) = 0$) implies that $F_1(0) = I_1(0) = F_A + F_S - \beta\sigma T_S^4$; using this together with equations (8) and (9) allows us to solve for $I_1(\tau)$:

$$I_1 = \left(F_S + F_A - \beta\sigma T_S^4\right)(1+\tau) - F_A\frac{\tau_0}{1+b}\left(\frac{\tau}{\tau_0}\right)^{b+1}. \tag{10}$$

The surface temperature, T_S, satisfies the boundary condition that $\sigma T_S^4 = F_1^-(\tau_0) + F_S$. Using $F_1^- = (I_1 - F_1)/2$ and the expressions for $I_1(\tau_0)$ and $F_1(\tau_0)$ from above yields

$$\sigma T_S^4 = \frac{F_S(2+\tau_0) + F_A\left(1 + \frac{b\tau_0}{b+1}\right)}{2 + \beta\tau_0}. \tag{11}$$

Now, returning to (7), we can solve for $B(\tau)$ and thus (from equation (6)) $T(\tau)$:

$$\sigma T^4(\tau) = \frac{\left(F_S + F_A - \beta\sigma T_S^4\right)(1+\tau) + \frac{F_A b}{\tau_0}\left(\frac{\tau}{\tau_0}\right)^{b-1} - \frac{F_A \tau_0}{b+1}\left(\frac{\tau}{\tau_0}\right)^{b+1}}{2(1-\beta)}. \quad (12)$$

We will return to the above expressions for surface and atmospheric temperature in equations (11) and (12) throughout the rest of this article (with equation (1) converting optical thickness to pressure).

There is generally a discontinuity in temperature at the surface: $T_S \neq T(\tau_0)$. A necessary condition for convective stability is that the surface be colder than the immediate overlying atmosphere. Combining equations (11) and (12) and simplifying gives:

$$\sigma T^4(\tau_0) - \sigma T_S^4 = \frac{F_A\left[\beta\left(1 + b + \frac{b\tau_0}{b+1}\right) + \frac{2b}{\tau_0}\right] - 2F_S(1-\beta)}{2(1-\beta)(2+\beta\tau_0)}. \quad (13)$$

In the no-window limit, $\beta = 0$, the surface is stable so long as total atmospheric heating exceeds a critical value: $F_A > \tau_0 F_S / b$. In general, radiative-advective equilibrium is stable to surface-based convection when the atmosphere is optically thin, when F_A is much larger than F_S, when atmospheric heating is bottom-heavy (i.e., b is large), and when the atmospheric window is large. Note that the surface discontinuity would in reality be smoothed out by boundary layer turbulence. Due to the high static stability, however, boundary layer turbulence would likely be weak, so a sharp near-surface inversion would remain.

3. Example Temperature Profiles

We plot example profiles to show how equations (11) and (12) depend on parameter choices, considering first the no-window limit, $\beta = 0$ (Figures 2a–2d). As in *Payne et al.* [2015], we use a reference state intended to represent the polar atmosphere in the annual-mean, with surface heating $F_S = 30$ W m^{-2}, atmospheric heating F_A=150 W m^{-2}, total optical thickness $\tau_0 = 3$, uniform heating in optical thickness ($b = 1$), and no window ($\beta = 0$). This state has emission temperature $T_e = \left[\sigma^{-1}(F_S + F_A)\right]^{1/4} \approx 237.4$ K, surface temperature $T_S = 260.8$ K, surface air temperature $T(\tau_0) = 263.2$ K, and a maximum logarithmic lapse rate $\mathrm{d}\log T/\mathrm{d}\log p \approx 0.18$, below the dry convective stability threshold of $R/c_p = 2/7$. The surface and interior of the atmosphere are thus both convectively stable. Increasing τ_0 gives warmer profiles throughout most but not all of the depth of the atmosphere and strongly warms the surface (Figure 2a). Increasing F_S warms the entire atmosphere but warms the lower troposphere and particularly the surface more than the upper troposphere (Figure 2b). Increasing F_A leads to near-uniform warming of the entire atmosphere and weaker warming of the surface (Figure 2c). Increasing b, corresponding to a more bottom-heavy distribution of atmospheric heating, steepens the atmospheric lapse rate but warms the lower troposphere more than the surface, strengthening the surface inversion. Decreasing b below 1 leads to a marked stratospheric inversion, because $Q_A(\tau) \to \infty$ as $\tau \to 0$ for $b < 1$ (Figure 2c). The only profile shown that is convectively unstable anywhere is the $b = 0.5$ case, which is superadiabatic at the surface.

What is the appropriate size of the window, β, for Earth? For clear skies and temperatures <300 K, the atmosphere is nearly transparent for wavelengths ~8–12 μm [*Pierrehumbert*, 2010]. The 8–12 μm range corresponds to about a quarter of the thermal emission from a blackbody with temperature 275 K and increases slightly with temperature. Thus, $\beta \approx 0.25$ seems reasonable for clear-sky conditions, though low atmospheric water vapor concentrations under cold conditions would open windows in other parts of the thermal spectrum. We use a somewhat smaller reference value of $\beta = 0.2$ to account for clouds, which lack significant infrared windows.

The most notable effects of a spectral window on our temperature profiles are to (1) reduce their sensitivity to changing τ_0, to (2) maintain stronger surface-based inversions under a broad range of conditions, and to (3) allow inversions within the lower troposphere itself rather than just at the surface (Figures 2e–2h). Increasing τ_0 with β fixed at 0.2 warms the surface and the lower troposphere but much less than in the case with no window (compare Figure 2e to Figure 2a). Furthermore, with our default parameters for (F_A, F_S, and b), a window with $\beta = 0.2$ means that no value of τ_0, no matter how large, can eliminate the atmospheric or surface-based inversions. The sensitivity of surface temperature to F_S and F_A is also weakened by the presence of a window, with much stronger surface-based inversions with $\beta = 0.2$ than with $\beta = 0$ (compare Figures 2f and 2g to

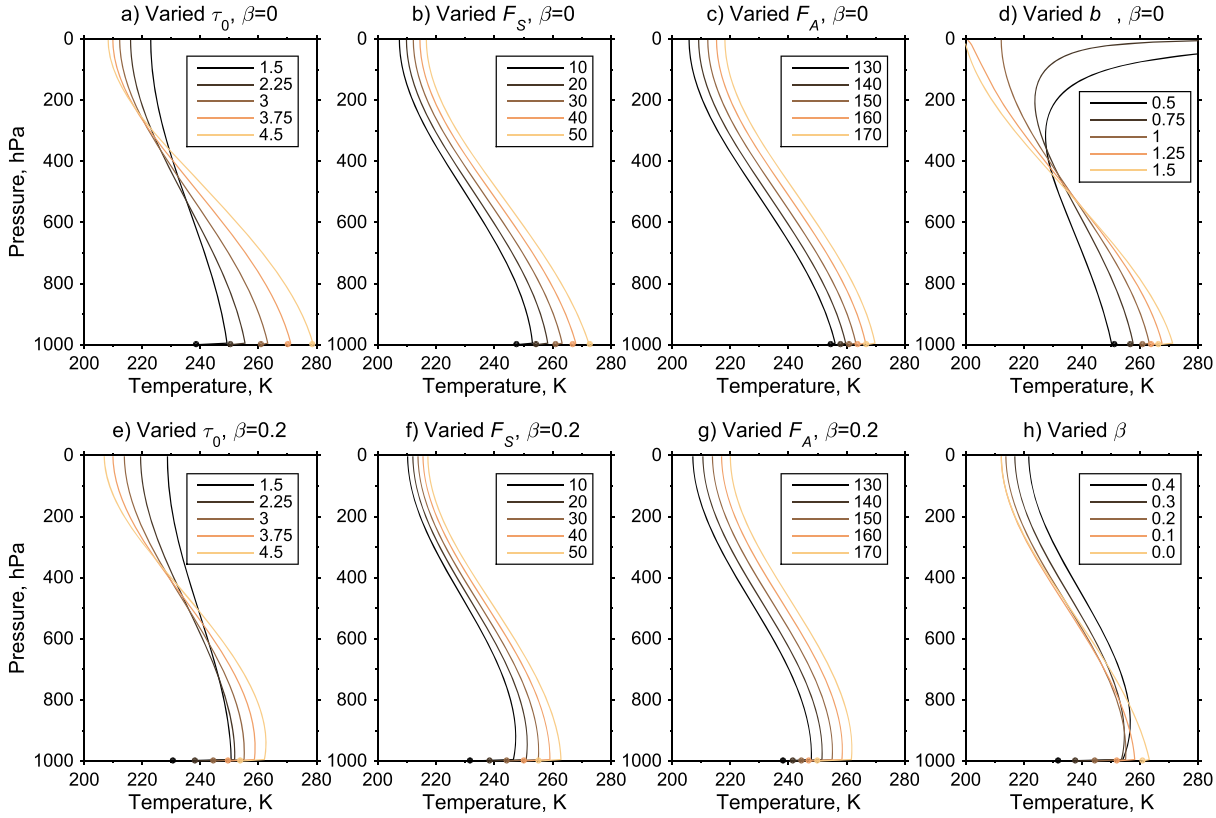

Figure 2. Example radiative-advective equilibrium temperature profiles, based on equations (11) and (12). Lines indicate atmospheric profiles and dots indicate surface temperatures. Default parameters are $F_S = 30$ W m^{-2}, $F_A = 150$ W m^{-2}, $\tau_0 = 3$, $b = 1$, and $\beta = 0$. (a–d) Solutions with no window, (e–g) solutions with $\beta = 0.2$, and (h) varied window width. In Figures 2a and 2e, τ_0 is varied from 1.5 to 4.5; in Figures 2b and 2f, F_S is varied from 10 to 50 W m^{-2}; in Figures 2c and 2g, F_A is varied from 130 to 170 W m^{-2}; in Figure 2d), b is varied: $b = 0.5$ corresponds to constant heating per unit pressure, and $b = 1$ corresponds to constant heating per unit optical thickness (linear in pressure).

Figures 2b and 2c). Increasing the width of the window always cools the surface and lowermost troposphere but can warm the atmosphere aloft by reducing its ability to emit to space (Figure 2h).

Because our solutions have been presented in optical thickness coordinates, it is simple to modify equation (1) to account for a different power law dependence of optical thickness on pressure. For example, larger values of $n \approx 4$ may be appropriate if the longwave absorption profile is controlled by water vapor partial pressure [*Weaver and Ramanathan*, 1995; *Frierson et al.*, 2006]. The response to such a change depends crucially on whether b is held constant (i.e., $Q_A(\tau)$ is held fixed—as may be justified if heat transport is also dominated by water vapor) or whether nb is held constant (i.e., $Q_A(p)$ is held fixed). If b is held constant, a shift to larger n tends to make profiles less convectively stable in their interiors and changes little else. If n is increased with nb held constant, however, the interior atmosphere generally becomes more stable, the surface temperature jump becomes less stable (or unstable), and the stratospheric temperature profiles show much stronger inversions.

4. Sensitivity to Forcing

We can directly compute the sensitivity of surface temperature to a small change in surface or atmospheric heating; we denote these sensitivities $\delta T_S/\delta F_S$ and $\delta T_S/\delta F_A$. Perturbation analysis of equation (11) yields

$$\frac{\delta T_S}{\delta F_S} = \frac{2 + \tau_0}{4\sigma T_S^3 (2 + \beta\tau_0)} \tag{14}$$

$$\frac{\delta T_S}{\delta F_A} = \frac{1 + \frac{b}{b+1}\tau_0}{4\sigma T_S^3 (2 + \beta\tau_0)}. \tag{15}$$

These expressions differ from each other by roughly a factor of two; the sensitivity of surface temperature to surface forcing is roughly twice as strong as the sensitivity to atmospheric forcing (this can also be seen in Figures 2b and 2c, and 2f and 2g). Equation (15) also shows that atmospheric heating is more effective at increasing surface temperature when b is large, and the heating is concentrated near the surface.

How does the sensitivity to radiative forcing caused by changing τ_0 compare to the cases of forcing by changing F_S and F_A? Answering this question requires calculating the radiative forcing, or change in top-of-atmosphere longwave radiation, δF_R, which is attributable to a small change $\delta\tau_0$, while holding the atmospheric and surface temperatures fixed at their equilibrium solutions for optical thickness τ_0:

$$\frac{\delta F_R}{\delta \tau_0} = - \left. \frac{F^+(0;\tau_0+\delta\tau_0) - F^+(0;\tau_0)}{\delta\tau_0} \right|_{T_S,T(p)}. \tag{16}$$

The top-of-atmosphere longwave flux, $F^+(0;\tau_0)$, can be written in terms of contributions from surface and atmospheric emission [*Pierrehumbert*, 2010]:

$$F^+(0;\tau_0) = \beta\sigma T_S^4 + (1-\beta)\left(\sigma T_S^4 e^{-\tau_0} + \int_0^{\tau_0} \sigma T^4(\tau') e^{-\tau'} \mathrm{d}\tau'\right), \tag{17}$$

Analytic evaluation of equations (17) and (16) is possible for integer b but leads to simple expressions for the radiative forcing only if $\beta = 0$ as well. Since the calculation even for this special case is algebraically cumbersome, we calculate radiative forcing by numerical integration. We obtain the sensitivity of surface temperature to radiative forcing as

$$\frac{\delta T_S}{\delta F_R} = \frac{(\delta T_S/\delta\tau_0)}{(\delta F_R/\delta\tau_0)}, \tag{18}$$

where the surface temperature sensitivity to increasing τ_0 is given from equation (11) as

$$\frac{\delta T_S}{\delta\tau_0} = \frac{2(1-\beta)F_S + \left(\frac{2b}{b+1} - \beta\right)F_A}{4\sigma T_S^3 (2+\beta\tau_0)^2}. \tag{19}$$

To demonstrate how the sensitivity to forcing varies, we plot surface temperature (T_S), surface temperature jump ($T(\tau_0) - T_S$), and all three sensitivities ($\delta T_S/\delta F_S$, $\delta T_S/\delta F_A$, and $\delta T_S/\delta F_R$) across a range of optical thicknesses τ_0 from 0.5 to 5, for both $\beta = 0$ (solid) and $\beta = 0.2$ (dashed) (Figure 3). Other control parameters are taken as in Figure 2. The surface temperature rises from roughly 220 K to 280 K across this range of optical thickness values for $\beta = 0$ but rises much less for $\beta = 0.2$. As τ_0 is increased, the surface temperature jump drops from a 40 K inversion to neutral stability for $\beta = 0$ and from a 55 K to a 10 K inversion for $\beta = 0.2$. The sensitivity of surface temperature to radiative forcing (from changing τ_0) is greatest, the sensitivity to surface heating is somewhat smaller, and the sensitivity to atmospheric heating is smaller still (Figure 3c). For small τ_0, $\delta T_S/\delta F_R$ diverges to infinity and then becomes negative (this branch is not shown). This divergence results from the radiative forcing δF_R crossing through zero and becoming negative for sufficiently small τ_0, because the atmosphere is warmer than the surface and increased atmospheric opacity leads to more top-of-atmosphere longwave emission. Although the radiative forcing switches signs (rendering sensitivity analysis confusing), the surface temperature increases monotonically with increasing optical thickness.

The ordering of sensitivities can also be interpreted in terms of climate feedbacks, particularly in terms of differences in the lapse rate feedback across forcings. We can write the sensitivity of surface temperature to forcing in terms of contributions from two feedbacks:

$$\delta T_S = -\frac{\delta F}{\lambda_P + \lambda_{LR}}, \tag{20}$$

where λ_P is the Planck feedback, or change in top-of-atmosphere energy balance for a vertically uniform warming of 1 Kelvin, and λ_{LR} is the lapse rate feedback, or change in top-of-atmosphere energy balance due to deviations from vertically uniform warming (the more the lapse rate steepens, the smaller the increase in outgoing longwave radiation per unit increase in surface temperature). Both feedbacks have units of W m^{-2} K^{-1}, and the sign convention on the feedbacks is that a negative signed feedback is stabilizing, and a positive signed feedback is destabilizing. In Figure 3d we show the Planck feedback, which is independent of type of

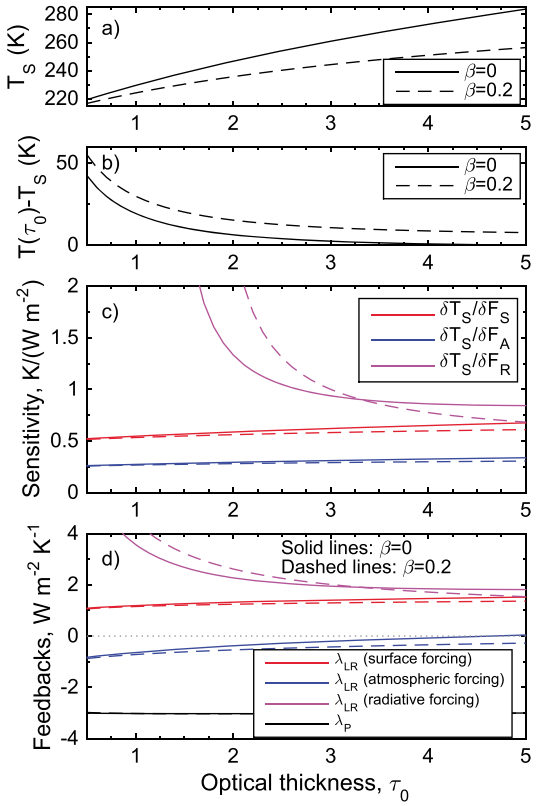

Figure 3. Sensitivity of radiative-advective equilibrium to forcing, across a range of τ_0 (0.5–5), for both $\beta = 0$ (solid lines) and $\beta = 0.2$ (dashed lines), with parameters F_S, F_A, and b as in Figure 2. (a) T_S as a function of τ_0, and (b) the surface temperature jump $T(\tau_0) - T_S$. (c) The sensitivity of surface temperature to surface forcing ($\delta T_S/\delta F_S$, red), atmospheric forcing ($\delta T_S/\delta F_A$, blue), and radiative forcing due to increasing τ_0 ($\delta T_S/\delta F_R$, magenta). (d) Decomposition of the total temperature feedback, $-\delta F/\delta T_S$, into a forcing-independent Planck feedback (black), and a forcing-dependent lapse rate feedback (red: surface forcing, blue: atmospheric forcing, and magenta: optical-thickness induced radiative forcing).

forcing, and the lapse rate feedback, which depends on the type of forcing. We calculate λ_P numerically, but it differs insignificantly from the approximation $\lambda_P \approx -4\sigma T_e^3 = -3.03\,\mathrm{W\,m^{-2}\,K^{-1}}$ here (recall $\sigma T_e^4 = F_S + F_A$); thus, λ_P is nearly independent of τ_0 as well. The lapse rate feedback is roughly $+2\,\mathrm{W\,m^{-2}\,K^{-1}}$ for radiative forcing (and decreases with τ_0), $+1.25\,\mathrm{W\,m^{-2}\,K^{-1}}$ for surface forcing, and weakly negative for atmospheric forcing. This ordering of lapse rate feedbacks can also be seen from the changes in lapse rate shown by Figure 2: atmospheric heating produces a nearly uniform warming, surface heating steepens the lapse rate somewhat, and increasing optical thickness steepens the lapse rate dramatically [as in *Payne et al.*, 2015].

5. Discussion and Conclusions

As in *Payne et al.* [2015], we have found that the high-latitude climate sensitivity depends on the nature of the forcing. One way to interpret the differing sensitivity to forcing is in terms of a forcing-dependent lapse-rate feedback. In contrast to the case of radiative-convective equilibrium, the lapse rate in radiative-advective equilibrium is not uniquely a function of the local surface temperature and thus not a "feedback" in the traditional sense. The nonunique lapse rate response to heating allows for complicated interactions between temperature feedbacks and additional feedbacks from clouds, water vapor, and surface albedo: just as each forcing above has its own lapse rate feedback, each additional feedback would activate a distinct lapse rate response. Thus, the total high-latitude lapse rate feedback in global models is likely a blend of lapse rate changes associated with many different processes, which vary in space and time and across models, and should not be thought of as a single mechanism. The nonuniqueness of the lapse rate feedback can also lead to pathological cases where a process or combination of processes alters the lapse rate and surface temperature with zero forcing at the top-of-atmosphere, seeming to imply infinite local sensitivity (consider a surface and

atmospheric heating dipole with $\delta F_S = -\delta F_A$). These points all indicate that caution is warranted when applying top-of-atmosphere forcing and feedback diagnostics to high-latitude climate change.

Our theory for the structure of the high-latitude atmosphere may be useful for understanding paleoclimate proxies and slow climate feedbacks, many of which are tied to the cryosphere. We emphasize that the local climate sensitivity to surface or radiative forcing is large, ~0.75 K per W m^{-2} of forcing (Figure 3c), making high-latitude surface temperatures sensitive to forcing by changing insolation or greenhouse gases even in the absence of amplification by albedo feedback or increasing moisture transport. Thus, slowly-evolving orbital and CO_2 forcing could have large effects on glacial mass balance, and a radiative-advective model could be useful for testing theories regarding ice age timing and high-latitude temperature on long time scales. For example, equation (11) could easily be used as a boundary condition for an ice-sheet model and would capture changes in surface temperature as an ice sheet accumulates (by scaling surface pressure and optical thickness).

The framework of radiative-advective equilibrium may also apply to understanding stable atmospheric regimes on other planets, in particular the permanently dark night side of tidally-locked rocky exoplanets. Nightside surface temperatures are important because of the potential for loss of all water—or even atmospheric collapse—to a nightside surface cold trap [*Menou*, 2013]. Recent work has shown that the interplay between radiative transfer and atmospheric heat transport from the dayside combine to determine the nightside surface temperature [*Koll and Abbot*, 2015; *Wordsworth*, 2015]. Our model could also be applied (with or without large-scale advection) to worlds with atmospheres that are relatively opaque to solar radiation but have a significant infrared window; *Mitchell* [2007] developed a similar model to ours to understand the stable troposphere of Titan but did not include Titan's atmospheric window region from ~400–600 cm^{-1} [*McKay et al.*, 1991].

The need to prescribe a heating profile is a significant limitation of this work. In reality, the advective heat flux convergence depends on meridional temperature and water vapor gradients, and the dynamics of stationary and transient eddies. A fully-developed theory for the high-latitude temperature structure and its sensitivity to forcing would need to incorporate a closure not only for the total heat flux convergence but also for its vertical structure. One approach to closing the problem of heat transport could be to relax temperatures toward a prescribed lower-latitude temperature profile. The approach of representing advection as relaxation to a known profile could help to merge the Eulerian perspective developed here with the Lagrangian perspective of cold air formation developed by previous studies (such studies have used a lower latitude temperature profile as an initial condition) [see *Wexler*, 1936; *Curry*, 1983; *Pithan et al.*, 2014; *Cronin and Tziperman*, 2015]. Although this approach may not lead to analytic solutions, including semiprognostic heat transport and more detailed physics could help to shed light on the potentially nonlinear [*Graversen et al.*, 2014] interactions among changing high-latitude surface albedo, heat transport, and lapse rate. Despite the limitation of fixed heat transport, we believe that the model described here advances our understanding of high-latitude climate sensitivity and that the framework of radiative-advective equilibrium provides a solid foundation for future work on polar climate.

Acknowledgments
We thank Tyler Robinson and one anonymous reviewer for constructive reviews and Peter Molnar for helpful comments on a draft of the manuscript. T.W.C. was supported by a NOAA Climate and Global Change Postdoctoral Fellowship and by the Harvard University Center for the Environment. This work began as two independent lines of inquiry and we thank Kyle Armour for suggesting collaboration. Processed data used in Figure 1 and Matlab scripts to make all figures are available at https://dl.dropboxusercontent.com/u/78078435/CJ15_RAE_grl.data.tar.

References

Abbot, D. S., and E. Tziperman (2008), Sea ice, high-latitude convection, and equable climates, *Geophys. Res. Lett.*, *35*, L03702, doi:10.1029/2007GL032286.

Chai, J., and G. K. Vallis (2014), The role of criticality on the horizontal and vertical scales of extratropical Eddies in a dry GCM, *J. Atmos. Sci.*, *71*, 2300–2318, doi:10.1175/JAS-D-13-0351.1.

Charney, J. G. (1947), The dynamics of long waves in a baroclinic westerly current, *J. Meteorol.*, *4*(5), 136–162.

Cronin, T. W., and E. Tziperman (2015), Low clouds suppress Arctic air formation and amplify high-latitude continental winter warming, *Proc. Natl. Acad. Sci.*, *112*, 11,490–11,495, doi:10.1073/pnas.1510937112.

Curry, J. (1983), On the formation of continental polar air, *J. Atmos. Sci.*, *40*(9), 2278–2292.

Frierson, D. M., I. M. Held, and P. Zurita-Gotor (2006), A gray-radiation aquaplanet moist GCM. Part I: Static stability and eddy scale, *J. Atmos. Sci.*, *63*, 2548–2566, doi:10.1175/JAS3753.1.

Graversen, R. G., P. L. Langen, and T. Mauritsen (2014), Polar amplification in CCSM4: Contributions from the lapse rate and surface albedo feedbacks, *J. Clim.*, *27*, 4433–4450, doi:10.1175/JCLI-D-13-00551.1.

Jansen, M. F., and R. Ferrari (2013), Equilibration of an atmosphere by adiabatic eddy fluxes, *J. Atmos. Sci.*, *70*, 2948–2962, doi:10.1175/JAS-D-13-013.1.

Kahl, J. D., and M. C. Serreze (2003), *Historical Arctic Rawinsonde Archive, All 70-80N Soundings From 1948-1996*, National Snow and Ice Data Center, Boulder, Colo., doi:10.5067/FQZA3330CVPO.

Kahl, J. D., M. C. Serreze, S. Shiotani, S. M. Skony, and R. C. Schnell (1992), In situ meteorological sounding archives for arctic studies, *Bull. Am. Meteorol. Soc.*, *73*, 1824–1830.

Koll, D. D. B., and D. S. Abbot (2015), Deciphering thermal phase curves of dry, tidally locked terrestrial planets, *Astrophys. J.*, *802*(21), 15, doi:10.1088/0004-637X/802/1/21.
McKay, C. P., J. B. Pollack, and R. Courtin (1991), The greenhouse and antigreenhouse effects on Titan, *Science*, *253*, 1118–1121.
Menou, K. (2013), Water-trapped worlds, *Astrophys. J.*, *774*(51), 8, doi:10.1088/0004-637X/774/1/51.
Mitchell, J. L. (2007), The climate dynamics of Titan, PhD thesis, 186 pp., The Univ. of Chicago, Chicago, Ill.
Overland, J. E., and P. S. Guest (1991), The Arctic snow and air temperature budget over sea ice during winter, *J. Geophys. Res.*, *96*(C3), 4651–4662.
Payne, A. E., M. F. Jansen, and T. W. Cronin (2015), Conceptual model analysis of the influence of temperature feedbacks on polar amplification, *Geophys. Res. Lett.*, *42*, 9561–9570, doi:10.1002/2015GL065889.
Pierrehumbert, R. (2010), *Principles of Planetary Climate*, Cambridge, U. K.
Pithan, F., and T. Mauritsen (2014), Arctic amplification dominated by temperature feedbacks in contemporary climate models, *Nat. Geosci.*, *7*, 181–184, doi:10.1038/NGEO2071.
Pithan, F., B. Medeiros, and T. Mauritsen (2014), Mixed-phase clouds cause climate model biases in Arctic wintertime temperature inversions, *Clim. Dyn.*, *43*, 289–303, doi:10.1007/s00382-013-1964-9.
Pollack, J. B. (1969), Temperature structure of nongray planetary atmospheres, *Icarus*, *10*, 301–313.
Robinson, T., and D. Catling (2012), An analytic radiative-convective model for planetary atmospheres, *Astrophys. J.*, *757*(1), 104, doi:10.1088/0004-637X/757/1/104.
Sobel, A. H., J. Nilsson, and L. M. Polvani (2001), The weak temperature gradient approximation and balanced tropical moisture waves, *J. Atmos. Sci.*, *58*, 3650–3665.
Stone, P. H. (1978), Baroclinic adjustment, *J. Atmos. Sci.*, *35*, 561–571.
Stone, P. H., and J. H. Carlson (1979), Atmospheric lapse rate regimes and their parameterization, *J. Atmos. Sci.*, *36*, 415–423.
Weaver, C. P., and V. Ramanathan (1995), Deductions from a simple climate model: Factors governing surface temperature and atmospheric thermal structure, *J. Geophys. Res.*, *100*, 11,585–11,591.
Wexler, H. (1936), Cooling in the lower atmosphere and the structure of polar continental air, *Mon. Weather Rev.*, *64*(4), 122–136.
Wordsworth, R. (2015), Atmospheric heat redistribution and collapse on tidally locked rocky planets, *Astrophys. J.*, *806*(180), 15, doi:10.1088/0004-637X/806/2/180.
Xu, K.-M., and K. A. Emanuel (1989), Is the tropical atmosphere conditionally unstable, *Mon. Weather Rev.*, *117*, 1471–1479.